

SEGMENTATION OF RIB BONES FROM MR DATA USING TRACKING APPROACH AND POLYNOMIAL PARAMETRIZATION

Harri Pölönen¹, Gerald Schubert²

¹VTT Technical Research Centre of Finland
Tampere, Finland
harri.polonen@vtt.fi

²Philips Healthcare
Vantaa, Finland

ABSTRACT

Segmentation of rib bones from magnetic resonance (MR) data is a challenging task due to the very weak MR signal of the bone tissue. The locations of the rib bones are indicated by the lack of signal between the surrounding soft tissues. We have developed an automated rib segmentation method, which tracks the bones from a given initial point using a pre-defined rib cross-section template. The three-dimensional location of the rib midline is parametrized with second order polynomials. The correct rib midline is determined through numerical optimization of polynomial parameters by maximizing cross-correlation between the template and the MR data. The segmentation result is a three-dimensional binary segmentation of the ribs, which can be output also as a surface. Comparison between the method's output and a manual segmentation shows that the method works adequately.

Index Terms— Magnetic resonance, segmentation, rib, HIFU

1. INTRODUCTION

Alongside established therapies, during the last decade MR-guided High Intensity Focused Ultrasound (HIFU) has emerged as a promising candidate for a non-invasively treating certain types of cancer [1, 2]. HIFU can be used to heat tissue in a well-defined target area. Exceeding a certain temperature threshold or sustaining a markedly elevated temperature during a sufficient amount of time results in necrosis or apoptosis and will finally kill the tumor cells. In MR-guided HIFU both treatment planning and non-invasive temperature monitoring are based on magnetic resonance imaging.

For a treatment of organs in the abdominal cavity (liver, pancreas, kidney) the ribs present a considerable obstacle for

the ultrasound beam. Blocking the beam path, the ribs hinder an efficient energy deposition in the target area. In addition, the higher absorption of ultrasound at the ribs can lead to tissue damage at their surface. It is therefore highly desirable to spare the ribs as far as possible from any exposure to ultrasound energy. In order to design efficient sonication strategies which avoid the ribs, a detailed knowledge of their position and shape is mandatory. In view of potential clinical application, rib detection should not rely on manual segmentation but be automated.

The fundamental problem in segmenting bones from MR data is that usually the bone tissue does not produce substantial amount of signal (See Fig.1). The situation gets even more challenging when the MR imaging sequence is set to maximize the contrast between soft tissues, cartilage and bone as is the case with HIFU therapy.

One way to solve this problem is to segment the bones from computerized tomography (CT) data of the respective patient, and thereafter register the CT data together with the segmented structures to the MR data. In CT data bones are clearly visible and there are several methods for segmentation [3, 4]. However, it has been reported that there may be significant health risks associated with acquiring whole-body CT data [5] and a possibility to avoid unnecessary CT scans would therefore be valuable.

Some methods have been developed for full thorax segmentation directly from MR data [6]. However, during the HIFU treatment process the patient is located inside the MR scanner and the segmentation needs to be a fast process. Registration of the whole thorax model may get unnecessary time-consuming. In addition, the actual field of view in MR scans during the treatment is limited to the, possibly very narrow, region of interest. Thus, there is a call for a simple and fast method to segment the bones from a partial MR view of the thorax.

In this study, we aim to develop a tracking-based rib segmentation method for MR data. We aim to model the rib

The study was (partly) supported by the SalWe Research Program for IMO (Tekes - the Finnish Funding Agency for Technology and Innovation grant 648/10).

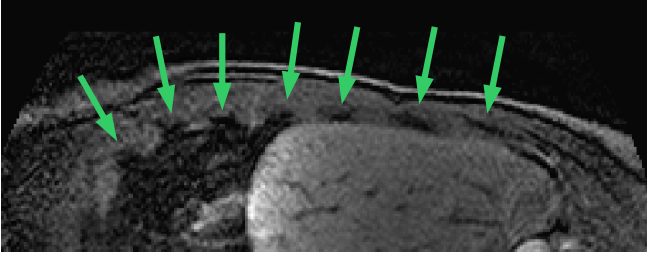


Fig. 1. Appearance of bones in MR data.

midline in three dimensions using polynomial parametrization and a pre-defined bone cross-section template. The estimated midline is then used to find the true cross-sectional profile of the bone and to construct a three-dimensional binary segmentation. The method is tested with real MR data and compared to manual segmentations.

2. METHODS AND MATERIALS

In our method the rib bone is segmented by tracking the rib midline from a given initial point $I = (I_x, I_y, I_z)$. The tracking is based on maximizing the correlation coefficient between the bone cross-section template and the MR data in the vicinity of the rib midline.

2.1. Rib midline model

The rib midline $R(s)$ is tracked parametrically with a model based on second order polynomials as

$$R(s) = \begin{pmatrix} R_x(s) \\ R_y(s) \\ R_z(s) \end{pmatrix} = \begin{pmatrix} a_x s^2 + b_x s + c_x \\ a_y s^2 + b_y s + c_y \\ a_z s^2 + b_z s + c_z \end{pmatrix}, \quad (1)$$

where $s \in [0, L]$ is determined in millimeter scale with L set as the desired length of the segmentation. By setting $R(0) = I$ it can be seen immediately that this determines the variables c_x, c_y and c_z leaving six parameters to be determined through numerical optimization. For simplicity these are denoted as $\theta = \{a_x, b_x, a_y, b_y, a_z, b_z\}$ from now on.

2.2. Computation of cross-sections

In order to determine the optimal rib midline, i.e. the optimal parameters θ , voxels in the vicinity of the rib midline are investigated. In our method, the normal planes of the rib midline are collected. When the rib midline is correctly estimated, these normal planes show cross-sections of the rib bone together with some surrounding tissues such as liver and subcutaneous fat/muscle (See Fig. 2).

To obtain the normal planes, we need to calculate which voxels in the MR data correspond to a specific normal plane. Because the rib midline is determined parametrically with

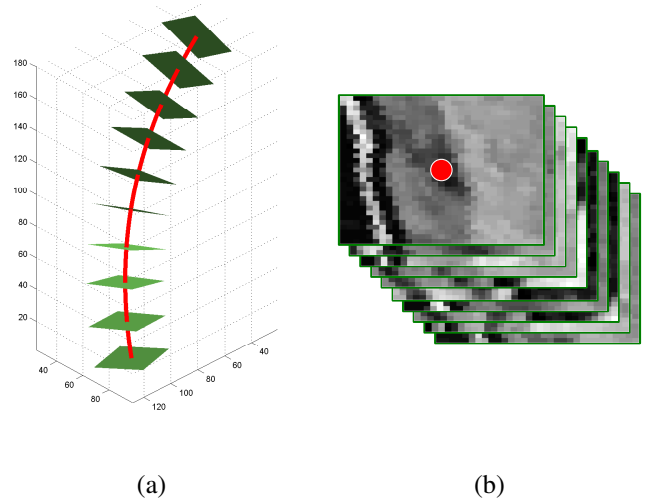


Fig. 2. (a) Visualization of polynomial rib midline and the planes normal to it. (b) The normal planes from the rib midline with the extracted voxel values from MR data. For better visualization the planes in (a) are more sparsely located than in real computations.

second order polynomials, it is straightforward to calculate the equations for the normal planes analytically. First, we calculate the tangent vector $\bar{g}(s|\theta)$ for the rib midline curve $R(s)$, which is defined simply with derivatives

$$\bar{g}(s|\theta) = \begin{pmatrix} \bar{g}_x(s|\theta) \\ \bar{g}_y(s|\theta) \\ \bar{g}_z(s|\theta) \end{pmatrix} = \begin{pmatrix} 2a_x s + b_x \\ 2a_y s + b_y \\ 2a_z s + b_z \end{pmatrix}. \quad (2)$$

The tangent vector \bar{g} is normalized to get the unit tangent vector g . Then the two unit vectors v and u that span the normal plane can be defined with the unit tangent vector as

$$v(s|\theta) = \begin{pmatrix} -\sqrt{1 - \frac{g_x(s|\theta)^2}{g_x(s|\theta)^2 + g_y(s|\theta)^2}} \\ \frac{g_x(s|\theta)}{\sqrt{g_x(s|\theta)^2 + g_y(s|\theta)^2}} \\ 0 \end{pmatrix} \quad (3)$$

and

$$u(s|\theta) = v(s|\theta) \times g(s|\theta), \quad (4)$$

where \times denotes the cross product of vectors.

The motivation for the seemingly cumbersome definition of vector v is that in this form v is always parallel to the axial slices. The non-zero components v_x and v_y are determined using the path gradient g and thus all the cross-section planes are aligned equally in relation to the path $R(s|\theta)$. If

the component v_z was not fixed, the definition of the normal planes would be ambiguous in terms of rotation around the path gradient. This in turn would cause problems when trying to match the fixed template to the normal planes.

In practice the actual vector values in a position s with parameters θ can be calculated just by inserting the parameter values to the above equations. This makes the computations very fast because the vector values are obtained with elementary numerical operations.

The voxels of the MR data V that correspond to the pixels of the normal planes $P(s|\theta)$ of the rib midline $R(s|\theta)$ are now obtained directly with the vectors u and v that span the normal planes as

$$P_{ij}(s|\theta) = V \begin{pmatrix} (i-n)v_x + (j-n)u_x + R_x \\ (i-n)v_y + (j-n)u_y + R_y \\ (j-n)u_z + R_z \end{pmatrix} \quad (5)$$

where i and j are running indices ($i, j = 0, \dots, 2n$) for pixels in plane $P(s)$. Note that in the above equation v , u and R depend on the parameters s and θ although they have been left out for notational simplicity and clarity.

2.3. Fitness function

The correct location of the rib is determined through numerical optimization of the parameters θ through the corresponding fitness function f . The fitness function is defined as the average sample correlation coefficient between pre-defined rib cross-section template T and the normal planes $P(s|\theta)$ extracted from the rib midline:

$$f(\theta) = \frac{1}{L+1} \sum_{t=0}^L \frac{Cov(P(s|\theta), T)}{\left((2n+1)^2 - 1 \right) \sigma(P(s|\theta)) \sigma(T)} \quad (6)$$

where $Cov()$ denotes the sample covariance and $\sigma()$ denotes the sample standard deviation. Note that $(2n+1)^2$ is equal to the number of pixels in the template T (and in each of the normal planes $P(s)$). The fitness function values are always within interval $[-1, 1]$ with values near ± 1 indicating high correlation and values near 0 showing lack of correlation.

The optimal parameters

$$\hat{\theta} = \arg \max_{\theta} f(\theta) \quad (7)$$

are determined with a purpose-built hybrid optimization method consisting of differential evolution algorithm [7] and Nelder-Mead simplex method [8].

2.4. Segmentation

After the rib midline has been successfully estimated by finding optimal parameters $\hat{\theta}$, the construction of the three-dimensional rib segmentation is straightforward. The planes $P(s|\hat{\theta})$ are averaged over s into a single two-dimensional

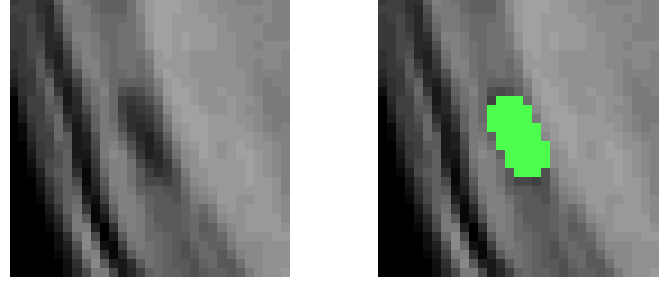


Fig. 3. Left: Average plane of the extracted normal planes. Right: The estimated bone cross-section overlaid on the average plane.

plane and the actual rib cross-section profile is found by fitting an ellipse to the average plane. A single ellipse can be fitted to the whole averaged data, because the planes are already mutually aligned due to the definition of normal vectors in Eq. (3) and Eq. (4).

The location of the ellipse within the average plane is fixed to the centre, while the ellipse rotation and the lengths of the major and minor axis are estimated (See Fig.3). Simply using the average voxel value difference between the ellipse interior and the ellipse exterior has turned out to be a well-working fitness function here. Because the range of anatomically feasible rib cross-section sizes is very limited, exhaustive search is used to find the best fitting ellipse. We used ellipse axis length range from 5 to 20 millimeters and maximum ellipse rotation of ± 30 degrees.

The binary three-dimensional bone segmentation is constructed first by setting voxels in the normal planes $P(s)$ to value 1 if the voxel is within the estimated ellipse and 0 otherwise. These binary normal planes are then back-projected to the three-dimensional space. From this three-dimensional binary segmentation it is possible to construct a surface if needed.

2.5. Data description

Images of a healthy volunteer were acquired on a clinical 1.5T MR-scanner (Achieva, Philips Healthcare). The 3D gradient echo sequence (Turbo Field Echo, TFE) is acquired using navigator-based respiratory gating. Sequence parameters (echo time TE=2ms, repetition time TR=4ms, flip angle FA=10°) are chosen to optimize the contrast between soft tissue and ribs/cartilage. Slice thickness is 2mm with 1mm slice spacing. Covering a field-of-view of 400mm the acquisition matrix size is 192 which results in a voxel size of 2.1mm. The MR slices were reconstructed into an isotropic volume with cubic voxels of size 1.5625mm using Insight ToolKit [9].

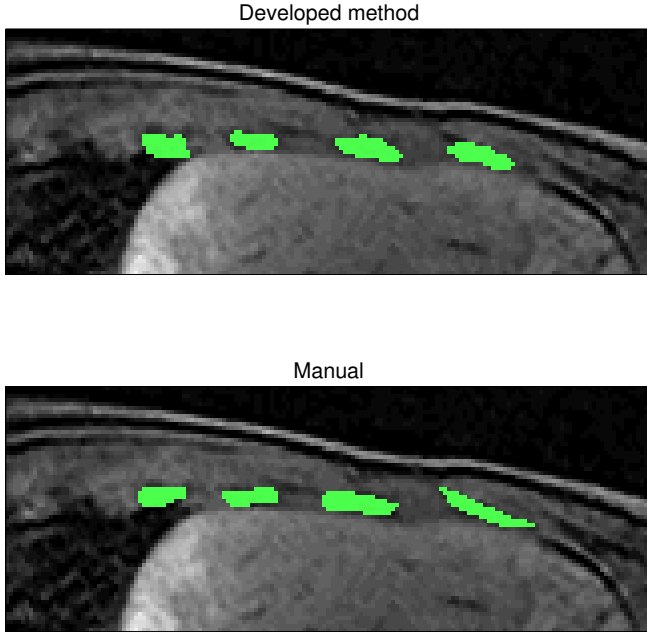


Fig. 4. Rib segmentation using the developed method and manual segmentation overlaid on a coronal slice of the MR data.

2.6. Dice index

The segmentation results are evaluated with Dice index d , which is calculated as ([10])

$$d = \frac{|D \cap M|}{\frac{1}{2}(|D| + |M|)}, \quad (8)$$

where D and M are binary segmentation volumes. Operator $|\cdot|$ gives the voxels in the corresponding segmented structure.

Dice index measures the similarity of two sets, or in this case, segmentations. Equation (8) gives the size of the union of two segmentations divided by their average size. Perfectly matching segmentations would yield a Dice index 1 and completely separate segmentation would give out a Dice index 0. It is not possible to declare a universally good Dice index level, because this depends strongly on the application in question, quality of the data and the nature of the used reference segmentation. As a rough estimate, at least values above 0.70 are expected for an adequate segmentation method but in some application even index values way above 0.95 can be achieved.

3. RESULTS

Numerical comparison between the output of the developed method and the expert manual segmentations can be seen in Table 1. The rib midline can be estimated with an average distance of 1.32 millimeters to the expert manual midline estimate. While the MR data voxels size in this test was 1.5625

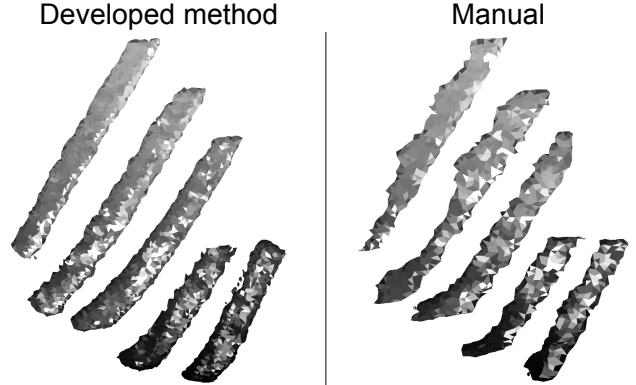


Fig. 5. Rib segmentation using the developed method and manual segmentation as surfaces.

millimeters, the result can be considered very good. The actual binary segmentations reach on average Dice index of 0.74, which is an acceptable but not an excellent value.

A coronal slice of the binary segmentations from the developed method and binary manual segmentations are presented in Fig. 4. It can be seen that visually the results match quite well with each other, although manual segmentation contains more variation in the bone shape. With the developed method the bone is always ellipse-shape in the direction of the normal plane and the actual bone shape is therefore rather limited.

Visualizations of the surface generated from the output from the developed method and the surface generated from the manual segmentation and can be seen in Fig. 5. The manual segmentation is rough and grainy because in many regions of the data there is no clear unambiguous gradient in the voxel values, which would indicate the exact location of the rib bone. For example in this MR data, air in the lungs produces very similar voxel values as the bone tissue. In addition, the manual segmentation is done on two-dimensional orthogonal planes which causes some inconsistency in three-dimensional shape. Thus, with the developed automated method the bone shape stays more consistent. Note that incomplete bone segments are shown because the bone are only partially in the MR imaging field of view.

4. CONCLUSION

We have presented a method to segment rib bones from MR data. The proof-of-concept results from experimental test shows that the method works adequately and is able to find the correct rib midline.

The comparison results against manual segmentation indicate that although the rib midline is found with very high accuracy, the weak spot in our method is the reconstruction of the binary segmentation volume. This may be partly due to the ellipse-shaped cross-section estimate, which is not per-

Rib no.	Average distance (mm)	Dice index
1	1.35	0.80
2	1.27	0.74
3	1.35	0.76
4	1.28	0.68
5	1.35	0.72
Average	1.32	0.74

Table 1. Numerical segmentation results. Average distance is calculated against the corresponding manually estimated rib midline. Dice index is calculated between binary segmentation given by the developed method and the binary manual segmentation.

fectly anatomically accurate. However, the bones in MR data appear often merely as noisy and irregular cavities in the surrounding tissues and it may not be possible to perform very reliable accurate segmentation anyway. In the future anatomically more correct templates should be tested though. It may also be worth testing if multiple templates could be used to conform the different segments of the bone and thus allow the segmented bone to get locally narrower or thicker.

In this paper we fixed the segmentation length a priori. However, it would be possible to implement an adaptive tracking method so that the tracking would be automatically stopped when the rib's end is met. As the fitness function values are always scaled to a fixed interval, a threshold could be determined for the fitness value to indicate that the rib should not be tracked any longer.

5. REFERENCES

- [1] James E. Kennedy, "High-intensity focused ultrasound in the treatment of solid tumours.," *Nat Rev Cancer*, vol. 5, no. 4, pp. 321–327, Apr 2005.
- [2] Ferenc A. Jolesz, Kullervo Hynynen, Nathan McDaniel, and Clare Tempny, "MR imaging-controlled focused ultrasound ablation: a noninvasive image-guided surgery.," *Magn Reson Imaging Clin N Am*, vol. 13, no. 3, pp. 545–560, Aug 2005.
- [3] Shanhui Sun, Christian Bauer, and Reinhard Beichel, "Automated 3-D segmentation of lungs with lung cancer in CT data using a novel robust active shape model approach.," *IEEE Trans Med Imaging*, vol. 31, no. 2, pp. 449–460, Feb 2012.
- [4] Shantanu Banik, Rangaraj M. Rangayyan, and Graham S. Boag, "Automatic segmentation of the ribs, the vertebral column, and the spinal canal in pediatric computed tomographic images.," *J Digit Imaging*, vol. 23, no. 3, pp. 301–322, Jun 2010.
- [5] David J. Brenner and Eric J. Hall, "Computed tomography—an increasing source of radiation exposure.," *N Engl J Med*, vol. 357, no. 22, pp. 2277–2284, Nov 2007.
- [6] B. P. Lelieveldt, R. J. van der Geest, M. R. Rezaee, J. G. Bosch, and J. H. Reiber, "Anatomical model matching with fuzzy implicit surfaces for segmentation of thoracic volume scans.," *IEEE Trans Med Imaging*, vol. 18, no. 3, pp. 218–230, Mar 1999.
- [7] Kenneth V. Price, Rainer M. Storn, and Jouni A. Lampinen, *Differential evolution - A practical approach to global optimization*, Springer, 2005.
- [8] Jeffrey C. Lagarias, James A. Reeds, Margaret H. Wright, and Paul E. Wright, "Convergence Properties of the Nelder–Mead Simplex Method in Low Dimensions.," *SIAM J. on Optimization*, vol. 9, no. 1, pp. 112–147, May 1998.
- [9] L. Ibanez, W. Schroeder, L. Ng, and J. Cates, *The ITK Software Guide*, Kitware, Inc. ISBN 1-930934-15-7, <http://www.itk.org/ItkSoftwareGuide.pdf>, second edition, 2005.
- [10] L. R. Dice, "Measures of the Amount of Ecologic Association Between Species," *Ecology*, vol. 26, no. 3, pp. 297–302, July 1945.